Optics Letters

Generation of hyper-entangled photons in a hot atomic vapor

CHENGYUAN WANG,[1,2,4] CHUNG-HYUN LEE,[2] YOSEP KIM,[2] AND YOON-HO KIM[2,3]

[1]Shaanxi Key Laboratory of Quantum Information and Quantum Optoelectronic Devices, School of Science, Xi'an Jiaotong University, Xi'an 710049, China
[2]Department of Physics, Pohang University of Science and Technology (POSTECH), Pohang, 37673, South Korea
[3]e-mail: yoonho72@gmail.com
[4]e-mail: wcy199202@gmail.com

Received 29 November 2019; revised 23 February 2020; accepted 26 February 2020; posted 26 February 2020 (Doc. ID 384567); published 19 March 2020

A source of hyper-entangled photons plays a vital role in quantum information processing, owing to its high information capacity. In this Letter, we demonstrate a convenient method to generate polarization and orbital angular momentum (OAM) hyper-entangled photon pairs via spontaneous four-wave mixing (SFWM) in a hot ^{87}Rb atomic vapor. The polarization entanglement is achieved by coherently combining two SFWM paths with the aid of two beam displacers that constitute a phase self-stabilized interferometer, and OAM entanglement is realized by taking advantage of the OAM conservation condition during the SFWM process. Our hyper-entangled biphoton source possesses high brightness and high nonclassicality and may have broad applications in atom–photon-interaction-based quantum networks.

https://doi.org/10.1364/OL.384567

An entangled photon source is crucial in quantum information protocols such as quantum teleportation [1–4]. The preparation of entangled photon pairs has become a hot topic in recent years, and biphoton entanglements have been reported for various degrees of freedom (DOFs) such as polarization [5–8], energy time [9–11], time bin [12], path [13], frequency [14], orbital angular momentum (OAM) [15,16], and Einstein–Podolsky–Rosen position momentum [17,18].

Hyper-entanglement refers to simultaneous entanglement in more than one DOF [19–21], which has the ability to coalesce and fully exert the advantages of each DOF and at the same time afford larger information capacity. Hence, hyper-entanglement possesses greater superiority and can be extensively exploited in superdense coding, Bell state analysis, quantum cryptography, and so on.

The generation of hyper-entangled photons is, to date, based mostly on a spontaneous parametric down-conversion (SPDC) process in nonlinear crystals [21]. But SPDC photons have a large bandwidth that cannot be utilized directly in atom–photon-interaction-based quantum networks. An alternative medium is the cold atom ensemble [22,23], which can generate narrow-bandwidth entangled photons that are suitable for quantum memory. Hyper-entangled photons in polarization and time–energy DOFs [24], and polarization and OAM DOFs [25] from cold atoms have been reported. However, cold atom systems are generally complex, bulky, and difficult to operate. Photon pairs generated in hot atomic ensembles [26,27] or optical fibers [28] by spontaneous four-wave mixing (SFWM) have been well studied lately due to the ease of implementation and low cost. But up to now, there is no work on generating hyper-entangled photons from the hot atomic ensemble.

In this Letter, we demonstrate, to the best of our knowledge, the first experimental realization of polarization-OAM hyper-entangled photon pairs in a hot ^{87}Rb atomic vapor cell via a ladder-type SFWM process. In our scheme, polarization entanglement is obtained by coherently combining bidirectional noncollinear SFWM photons via two beam displacers (BDs) [29], while OAM entanglement is obtained by the OAM conservation condition among input beams and output biphotons during the SFWM process. The generation rate and nonclassicality of the photon pairs are very high due to the collective two-photon coherence effect in the Doppler-broadened ladder-type atomic system [30]. The polarization-OAM hyper-entangled state is verified by conducting quantum state tomography, which shows high fidelity compared to the ideal entangled state. Also, our biphoton source naturally possesses time–energy entanglement [9] and Einstein–Podolsky–Rosen entanglement [17]. Integrating these with the polarization-OAM DOFs can achieve the superhigh-dimensional hyper-entangled state, which may have many potential applications in optical quantum information processing.

The schematic experimental setup is shown in Fig. 1. A 20-mm-long rubidium cell heated to 60°C is used for generating hyper-entangled photon pairs via a ladder-type SFWM process. The pump beam (780 nm, ω_p) having vertical polarization and 1 mW power is blue detuned from $|5S_{1/2}, F=2\rangle \rightarrow |5P_{3/2}, F'=3\rangle$ by 1 GHz, while the coupling beam (776 nm, ω_c) having vertical polarization and 9 mW power is red detuned from $|5P_{3/2}, F'=3\rangle \rightarrow |5D_{5/2}, F''=4\rangle$ by 1 GHz. The frequencies of these two lasers satisfy the $|5S_{1/2}, F=2\rangle \rightarrow |5D_{5/2}, F''=4\rangle$ two-photon resonant

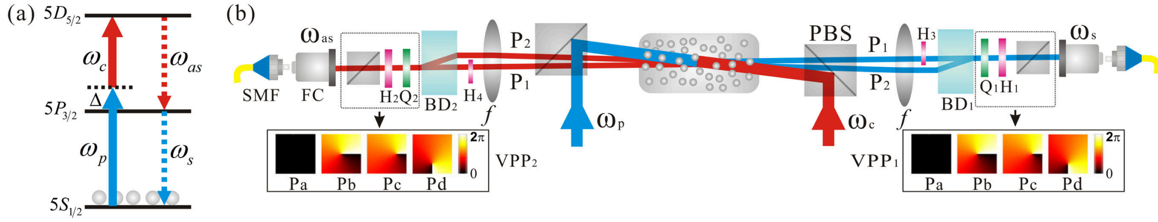

Fig. 1. (a) Energy level and (b) experimental setup for generating hyper-entangled photon pairs. SMF, single-mode fiber; FC, fiber collimator; PBS, polarizing beam splitter; H, half-wave plate; Q, quarter-wave plate; f, lens with focal length of $f = 400$ mm; VPP, vortex phase plate; P_a, P_b, P_c, and P_d are the phase patterns of the VPP for measuring $|G\rangle$, $|R\rangle$, $1/\sqrt{2}(|G\rangle + |R\rangle)$, and $1/\sqrt{2}(|G\rangle - i|R\rangle)$ modes, respectively; BD, beam displacer.

condition [9]. The pump beam and coupling beam are collinear and counter-propagating with each other. Horizontally polarized anti-Stokes photons (776 nm, ω_{as}) and Stokes photons (780 nm, ω_s) are spontaneously generated from path 1 (P_1) and path 2 (P_2) in the phase-matched direction and are collected with a 1.5° angle relative to the pump and coupling beams. Two half-wave plates H_3 and H_4 are set at 45° and put in P_1 to convert the ω_{as} and ω_s photons into vertical polarization. Biphotons from P_1 and P_2 are then perfectly overlapped by BD_1 and BD_2 after aligned in parallel propagation by means of two lenses (f) placed at distances of 400 mm relative to the center of the atomic cell. This structure can form a phase-insensitive interferometer, and there is no need to lock the phase between the two paths [29]. With this setup, we successfully generate hyper-entangled photon pairs in the polarization and OAM DOFs. The basic principles are described in detail below.

First let us concentrate on the generation of polarization entanglement. There are several common methods to generate atomic-ensemble-based polarization entangled biphotons. For instance, taking advantage of multiple spin angular momentum (SAM) transition channels during the SFWM process [25] can directly generate a polarization entangled state. But this method generally generates a non-maximum entangled state due to the asymmetric transition channels. Utilizing right-angle geometry between pump lasers and SFWM biphotons [24] can generate a maximum entangled state. However, large pump beam power is needed, and the photons' generation rates are relatively low in such schemes. Combining two separate SFWM pathways with a Mach–Zehnder interferometer [5,31] can efficiently generate a maximum entangled state, but this scheme needs an additional laser to retain phase stability, which adds to the system complexity. Recently, Yu *et al.* successfully generated polarization entangled biphotons from the cold atomic ensemble by using two BDs to combine two separate SFWM pathways. There is no need to lock the phase between two SFWM biphoton propagation paths on account of the symmetrical structure [29]. In this work, we adopt this method for the polarization entanglement preparation.

As shown in Fig. 1, horizontally polarized photon pairs transmit through the two polarizing beam splitters (PBSs), while vertically polarized photons are reflected and filtered by PBSs. The polarization DOF biphoton states after the PBSs can be expressed as $|\psi\rangle_{P_1} = |H\rangle_{\text{as},P_1}|H\rangle_{s,P_1}$ and $|\psi\rangle_{P_2} = |H\rangle_{\text{as},P_2}|H\rangle_{s,P_2}$. We change both the ω_{as} photons and ω_s photons in P_1 to vertical polarization by setting H_3 and H_4 at a 45° angle, then make P_1 and P_2 coherently superposed by BD_1 and BD_2. Thus, after the two BDs, the polarization entangled state is generated as

$$|\psi\rangle_{\text{Polarization}} = \frac{1}{\sqrt{2}}\left(|H_s H_{\text{as}}\rangle + e^{2ik\Delta x}|V_s V_{as}\rangle\right), \quad \textbf{(1)}$$

where $k = 2\pi/\lambda$, and Δx is the transverse optical path difference between P_1 and P_2. If we adjust BD_1 or BD_2 to set $e^{2ik\Delta x}$ to 1 or -1, $|\psi^+\rangle = \frac{1}{\sqrt{2}}(|H_s H_{\text{as}}\rangle + |V_s V_{\text{as}}\rangle)$ and $|\psi^-\rangle = \frac{1}{\sqrt{2}}(|H_s H_{\text{as}}\rangle - |V_s V_{\text{as}}\rangle)$ can be generated. Meanwhile, if we place H_3 or H_4 to P_2 and alter the two BDs, another two bell states, $|\phi^+\rangle = \frac{1}{\sqrt{2}}(|H_s V_{\text{as}}\rangle + |V_s H_{\text{as}}\rangle)$ and $|\phi^-\rangle = \frac{1}{\sqrt{2}}(|H_s V_{\text{as}}\rangle - |V_s H_{\text{as}}\rangle)$, can be obtained as well.

To generate an ideal polarization entangled state, the bidirectional noncollinear SFWM paths should be overlapped perfectly after the two BDs and the single mode fiber (SMF) coupling efficiencies for P_1 and P_2 should be the same. We achieve 65% fiber–fiber coupling efficiency for both P_1 and P_2 and then measure the two paths' coincidence counts between ω_{as} and ω_s photons separately. Figure 2 shows the coincidence counts in 40 s with time-bin width $\Delta t_{\text{bin}} = 196$ ns for P_1 and P_2. The waveform likeness L [32] can be used to characterize waveform similarity and is calculated as $L = \frac{|\sum\sqrt{N_{P1}(\tau)N_{P2}(\tau)}|^2}{\sum|\sqrt{N_{P1}(\tau)}|^2 \times \sum|\sqrt{N_{P2}(\tau)}|^2}$, where $N_{P1/P2}(\tau)$ is the coincidence value at time τ. Biphoton waveform likeness between Figs. 2(a) and 2(b) is $L = 98.8\%$, indicating that the amplitudes between the $|HH\rangle$ and $|VV\rangle$ components in Eq. (1) are balanced. The maximum cross-correlation functions $g^{(2)}_{s,\text{as}}(\tau)$ for both paths are measured to be 250 ± 16. Supposing the autocorrelation functions for both ω_s and ω_{as} photons are $g^{(2)}_{s,s}(0) = g^{(2)}_{\text{as,as}}(0) = 2$ [5], we can obtain $[g^{(2)}_{s,\text{as}}(\tau)]^2/[g^{(2)}_{s,s}(0)g^{(2)}_{\text{as,as}}(0)] = (1.56 \pm 0.39) \times 10^4$. This value strongly violates the Cauchy–Schwarz inequality $[g^{(2)}_{s,\text{as}}(\tau)]^2/[g^{(2)}_{s,s}(0)g^{(2)}_{\text{as,as}}(0)] \leq 1$ and manifests the high

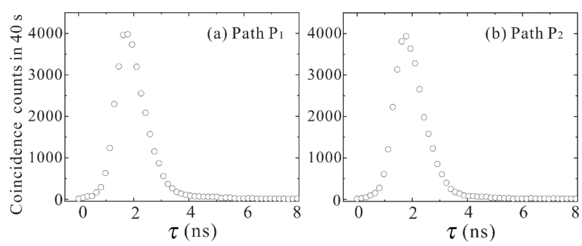

Fig. 2. Coincidence counts are measured with 40 s collection time for path 1 (2) when path 2 (1) is blocked. τ represents the relative time delay between anti-Stokes photons and Stokes photons. The cross-correlation functions for both paths are 250 ± 16, which violate the Cauchy–Schwarz inequality by a factor of $(1.56 \pm 0.39) \times 10^4$, indicating the high nonclassicality of the biphoton source. The biphoton waveform likeness between (a) and (b) is 98.8%.

nonclassicality of our biphoton source. From the data, we can also see that the photon pair's generation rate is about 7000 pairs/s (considering the total collection efficiency of about 20% in our system). The high photon pair generation rate of such a SFWM process is due to the superradiant effect in the Doppler-broadened atomic ensemble [30].

After noting that the two paths' biphotons are identical, we adjust BD_2 to set $e^{2ik\Delta x} = 1$ or $e^{2ik\Delta x} = -1$ in Eq. (1). Then we can obtain two polarization entangled states:

$$|\psi^+\rangle_{\text{Polarization}} = \frac{1}{\sqrt{2}}\left(|H_s H_{as}\rangle + |V_s V_{as}\rangle\right), \tag{2}$$

$$|\psi^-\rangle_{\text{Polarization}} = \frac{1}{\sqrt{2}}\left(|H_s H_{as}\rangle - |V_s V_{as}\rangle\right). \tag{3}$$

OAM entanglement of the photon pairs is illustrated in the following. In general, a light beam carrying OAM can be described by the Laguerre–Gaussian (LG_{PL}) function under cylindrical coordinates. Here P (L) refers to the radial (azimuthal) number. In our experiment, we consider only the case of $P = 0$ (LG_{0L}). During the SFWM process, the total OAM among input beams and output biphotons should be conserved [16], i.e.,

$$m_p + m_c = m_s + m_{as}, \tag{4}$$

where m_p, m_c, m_s, and m_{as} represent OAM values for pump beam, coupling beam, ω_s photons, and ω_{as} photons, respectively. If $m_p = m_c = 0$, the biphotons generated by SFWM will be in the OAM entangled state

$$|\Psi\rangle = C \sum_{m=-\infty}^{+\infty} \gamma_m |m_s\rangle |m_{as}\rangle, \tag{5}$$

where C is the normalized coefficient, and γ_m is the relative weight of different OAM states.

In our experiment, both pump and coupling beams carry zero OAM ($m_p = m_c = 0$). For simplicity, we consider only $m_s = 0$ and $m_s = 1$ modes for the ω_s photons and $m_{as} = 0$ and $m_{as} = -1$ modes for the ω_{as} photons. G, R, and L are used in the following to represent the OAM states 0, $\hbar$, and $-\hbar$, respectively. Thus, the two-dimensional OAM entangled state can be written as

$$|\psi\rangle_{\text{OAM}} = \frac{1}{\sqrt{1+\alpha_1^2}}\left(|G_s G_{as}\rangle + \alpha_1 |R_s L_{as}\rangle\right). \tag{6}$$

Because the ω_s and ω_{as} photons are counter-propagating, it is more convenient to express the OAM state in two detectors' reference frames, and then Eq. (6) can be rewritten as

$$|\psi\rangle'_{\text{OAM}} = \frac{1}{\sqrt{1+\alpha_1^2}}\left(|G_s G_{as}\rangle + \alpha_1 |R_s R_{as}\rangle\right). \tag{7}$$

To sum up, the biphoton source in our scheme is therefore in the polarization-OAM hyperentangled state

$$|\psi\rangle = |\psi^\pm\rangle_{\text{Polarization}} \otimes |\psi\rangle'_{\text{OAM}}. \tag{8}$$

To completely characterize the entangled states, we conduct quantum state tomography with the maximum likelihood estimation method to determine the density matrices for both polarization DOFs and OAM DOFs.

As shown in Fig. 1, four wave plates (Q_1, H_1, Q_2, H_2) and two PBSs are placed at ω_s and ω_{as} collection paths to execute quantum state tomography measurement in the polarization DOF. We obtain 16 values (each value is from the total coincidence counts with 4 ns coincidence window in 30 s collection time) by projecting each photon into the four bases: $|H\rangle$, $|V\rangle$, $|D\rangle = 1/\sqrt{2}(|H\rangle + |V\rangle)$, and $|R\rangle = 1/\sqrt{2}(|H\rangle - i|V\rangle)$. Figure 3 is the graphical representation of the reconstructed density matrix, where (a) and (b) show the real and imaginary parts, respectively, of $|\psi^+\rangle_{\text{Polarization}}$, while (c) and (d) are the real and imaginary parts, respectively, of $|\psi^-\rangle_{\text{Polarization}}$. From the reconstructed density matrix ρ_0, the fidelity $\text{F} = \text{Tr}(\sqrt{\sqrt{\rho_1}\rho_0\sqrt{\rho_1}})^2$ compared to the corresponding maximally entangled state ρ_1 can be calculated. We obtain a fidelity of 95.8% (95.7%) for $|\psi^+\rangle_{\text{Polarization}}$ ($|\psi^-\rangle_{\text{Polarization}}$) to the ideal Bell state $|\Psi^+\rangle = \frac{1}{\sqrt{2}}(|HH\rangle + |VV\rangle)$ ($|\Psi^-\rangle = \frac{1}{\sqrt{2}}(|HH\rangle - |VV\rangle)$). The biphotons are entangled when the concurrence (C) value satisfies the $0 < C \le 1$ condition [33]. From the corresponding density matrix, we obtain $C = 0.925 \pm 0.005$ for $|\psi^+\rangle_{\text{Polarization}}$ and $C = 0.951 \pm 0.004$ for $|\psi^-\rangle_{\text{Polarization}}$. From the results above, we confirm that our biphoton source is polarization entangled.

To verify OAM entanglement, we also perform quantum-state tomography by projecting each photon in different OAM measurement bases with the aid of vortex phase plates (VPPs) (VPP-1b, RPC Photonics Corp.) and SMFs. The four measurement bases are chosen as $|G\rangle$, $|R\rangle$, $1/\sqrt{2}(|G\rangle + |R\rangle)$, and $1/\sqrt{2}(|G\rangle - i|R\rangle)$. The phase patterns for measuring these four bases are shown in Fig. 1 as P_a, P_b, P_c, and P_d, correspondingly [34]. The margin area of the VPP containing no phase (P_a pattern) can be employed to measure the $|G\rangle$ mode. The center of the VPP (P_b pattern), where the phase singularity

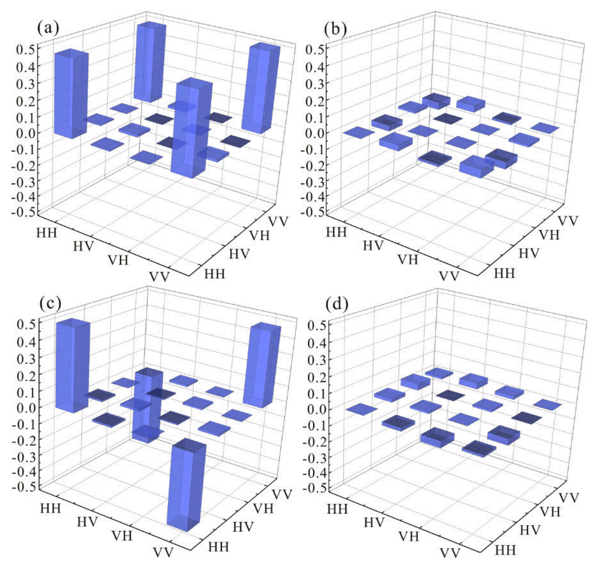

Fig. 3. Reconstructed density matrix for polarization entangled states $|\psi^+\rangle_{\text{Polarization}}$ and $|\psi^-\rangle_{\text{Polarization}}$. (a), (b) Real part and imaginary part, respectively, of $|\psi^+\rangle_{\text{Polarization}}$; (c), (d) real part and imaginary part, respectively of $|\psi^-\rangle_{\text{Polarization}}$. The fidelity of $|\psi^+\rangle_{\text{Polarization}}$ ($|\psi^-\rangle_{\text{Polarization}}$) to the ideal Bell state $|\Psi^+\rangle = \frac{1}{\sqrt{2}}(|HH\rangle + |VV\rangle)$ ($|\Psi^-\rangle = \frac{1}{\sqrt{2}}(|HH\rangle - |VV\rangle)$) is measured to be 95.8 % (95.7 %). All experimental data are raw data without error corrections.

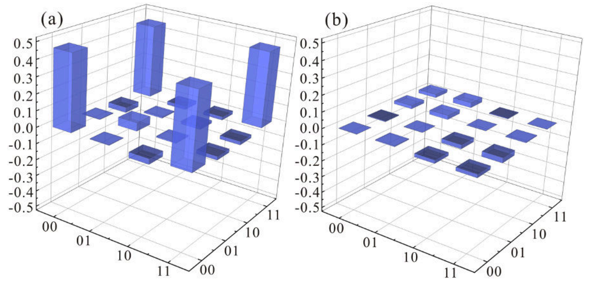

Fig. 4. Reconstructed density matrix for the OAM entangled state $|\psi\rangle'_{\mathrm{OAM}}$. The real and imaginary parts are shown in (a) and (b), respectively. The fidelity of $|\psi\rangle'_{\mathrm{OAM}}$ to the ideal Bell state $|\Psi\rangle = (|GG\rangle + |RR\rangle)/\sqrt{2}$ is measured to be 91.9%. All experimental data are raw data without error corrections.

locates, is used for measuring the $|R\rangle$ mode. The superposition base $1/\sqrt{2}(|G\rangle + |R\rangle)$ is measured by shifting the VPP (P_c pattern), while $1/\sqrt{2}(|G\rangle - i|R\rangle)$ can be measured by shifting and rotating the VPP (P_d pattern). Figure 4 shows the reconstructed density matrix from 16 coincidence counts under the combinations of the four measurement bases. We obtain a fidelity of 91.9% compared to the maximally entangled state $|\Psi\rangle = (|GG\rangle + |RR\rangle)/\sqrt{2}$. For $|\psi\rangle'_{\mathrm{OAM}}$, $C = 0.875 \pm 0.005$ is obtained from the reconstructed density matrix. The parameter $\alpha_1 = \gamma_1/\gamma_0$ is estimated as 0.9 here (γ_0 and γ_1 are the total coincidence counts of $|GG\rangle$ and $|RR\rangle$ components, respectively). In addition, this parameter could be further adjusted by changing the spatial modes of pump and coupling beams and altering the positions of the collection lenses, which can influence the generation rates and collection efficiencies of different OAM modes.

In conclusion, we demonstrate, as far as we know, the first generation of polarization-OAM hyper-entangled photon pairs via ladder-type SFWM in a hot ^{87}Rb atomic ensemble. In our scheme, polarization entanglement is realized by the combination of two SFWM paths with the aid of two BDs, while OAM entanglement is achieved by taking advantage of the total OAM conservation during the SFWM process. The polarization-OAM hyper-entangled state is verified by conducting quantum state tomography, which shows high fidelity compared to the ideal entangled state. The hyper-entangled photon pair source in our scheme has a very high generation rate and high nonclassicality. Also, the photon's bandwidth is much narrower compared with the SPDC source, and the system configuration is much simpler than cold atom experiments. Hence, our hyper-entangled photon source can be applied widely to the atomic-ensemble-based quantum information and quantum communication protocols. It has been shown that this kind of biphoton source naturally possesses time–energy entanglement [9] and Einstein–Podolsky–Rosen entanglement [17,18]. Combining these two with the polarization-OAM DOFs can achieve a multidimensional hyper-entangled state, which may have broad applications in practical scalable quantum networks.

Funding. National Research Foundation of Korea (2019R1A2C3004812); National Natural Science Foundation of China (11534008, 11774286).

Disclosures. The authors declare no conflicts of interest.

REFERENCES

1. C. H. Bennett, G. Brassard, C. Crépeau, R. Jozsa, A. Peres, and W. K. Wootters, Phys. Rev. Lett. **70**, 1895 (1993).
2. D. Bouwmeester, J.-W. Pan, K. Mattle, M. Eibl, H. Weinfurter, and A. Zeilinger, Nature **390**, 575 (1997).
3. D. Boschi, S. Branca, F. De Martini, L. Hardy, and S. Popescu, Phys. Rev. Lett. **80**, 1121 (1998).
4. Y.-H. Kim, S. P. Kulik, and Y. Shih, Phys. Rev. Lett. **86**, 1370 (2001).
5. K. Liao, H. Yan, J. He, S. Du, Z.-M. Zhang, and S.-L. Zhu, Phys. Rev. Lett. **112**, 243602 (2014).
6. M.-X. Dong, W. Zhang, Z.-B. Hou, Y.-C. Yu, S. Shi, D.-S. Ding, and B.-S. Shi, Opt. Lett. **42**, 4691 (2017).
7. P. G. Kwiat, K. Mattle, H. Weinfurter, A. Zeilinger, A. V. Sergienko, and Y. Shih, Phys. Rev. Lett. **75**, 4337 (1995).
8. Y.-H. Kim, S. P. Kulik, M. V. Chekhova, W. P. Grice, and Y. Shih, Phys. Rev. A **67**, 010301 (2003).
9. J. Park, D. Kim, H. Kim, and H. S. Moon, Opt. Lett. **44**, 3681 (2019).
10. Y.-W. Cho, K.-K. Park, J.-C. Lee, and Y.-H. Kim, Phys. Rev. Lett. **113**, 063602 (2014).
11. K.-K. Park, J.-H. Kim, T.-M. Zhao, Y.-W. Cho, and Y.-H. Kim, Optica **4**, 1293 (2017).
12. P. Farrera, G. Heinze, and H. de Riedmatten, Phys. Rev. Lett. **120**, 100501 (2018).
13. Y.-S. Kim, O. Kwon, S. M. Lee, J.-C. Lee, H. Kim, S.-K. Choi, H. S. Park, and Y.-H. Kim, Opt. Express **19**, 24957 (2011).
14. X. Guo, P. Chen, C. Shu, M. M. T. Loy, and S. Du, J. Opt. **17**, 105201 (2015).
15. A. Mair, A. Vaziri, G. Weihs, and A. Zeilinger, Nature **412**, 313 (2001).
16. Q.-F. Chen, B.-S. Shi, Y.-S. Zhang, and G.-C. Guo, Phys. Rev. A **78**, 053810 (2008).
17. J.-C. Lee, K.-K. Park, T.-M. Zhao, and Y.-H. Kim, Phys. Rev. Lett. **117**, 250501 (2016).
18. C. Wang, C.-H. Lee, and Y.-H. Kim, Opt. Express **27**, 34611 (2019).
19. M.-X. Dong, W. Zhang, S. Shi, K. Wang, Z.-Y. Zhou, S.-L. Liu, D.-S. Ding, and B.-S. Shi, Opt. Express **25**, 10145 (2017).
20. C. Shu, X. Guo, P. Chen, M. M. T. Loy, and S. Du, Phys. Rev. A **91**, 043820 (2015).
21. J. T. Barreiro, N. K. Langford, N. A. Peters, and P. G. Kwiat, Phys. Rev. Lett. **95**, 260501 (2005).
22. W. Zhang, D.-S. Ding, M.-X. Dong, S. Shi, K. Wang, S.-L. Liu, Y. Li, Z.-Y. Zhou, B.-S. Shi, and G.-C. Guo, Nat. Commun. **7**, 13514 (2016).
23. K.-K. Park, Y.-W. Cho, Y.-T. Chough, and Y.-H. Kim, Phys. Rev. X **8**, 021016 (2018).
24. H. Yan, S. Zhang, J. F. Chen, M. M. T. Loy, G. K. L. Wong, and S. Du, Phys. Rev. Lett. **106**, 033601 (2011).
25. T.-M. Zhao, Y. S. Ihn, and Y.-H. Kim, Phys. Rev. Lett. **122**, 123607 (2019).
26. C. Shu, P. Chen, T. K. A. Chow, L. Zhu, Y. Xiao, M. M. T. Loy, and S. Du, Nat. Commun. **7**, 12783 (2016).
27. C. Wang, Y. Gu, Y. Yu, D. Wei, P. Zhang, H. Gao, and F. Li, Chin. Opt. Lett. **16**, 082701 (2018).
28. J.-H. Kim, Y. S. Ihn, Y.-H. Kim, and H. Shin, Opt. Lett. **44**, 447 (2019).
29. Y. C. Yu, D.-S. Ding, M.-X. Dong, S. Shi, W. Zhang, and B.-S. Shi, Phys. Rev. A **97**, 043809 (2018).
30. J. Park, T. Jeong, H. Kim, and H. S. Moon, Phys. Rev. Lett. **121**, 263601 (2019).
31. D.-S. Ding, W. Zhang, Z.-Y. Zhou, S. Shi, B.-S. Shi, and G.-C. Guo, Nat. Photonics **9**, 332 (2015).
32. J. Li, J. Li, Y. Wang, S. Zhang, J. He, A. Cheng, H. Yan, and S.-L. Zhu, "High efficiency quantum storage of single photons in cold atoms," arXiv:1706.01404 (2017).
33. V. Coffman, J. Kundu, and W. K. Wootters, Phys. Rev. A **61**, 052306 (2000).
34. Z.-Q. Zhou, Y.-L. Hua, X. Liu, G. Chen, J.-S. Xu, Y.-J. Han, C.-F. Li, and G.-C. Guo, Phys. Rev. Lett. **115**, 070502 (2015).